An Improved Deadbeat Predictive Current Control Scheme for Open-Winding Permanent Magnet Synchronous Motors Drives With Disturbance Observer

Xueping Li, Shuo Zhang, *Member, IEEE*, Chengning Zhang, Ying Zhou, and Chuntao Zhang

***Abstract*—To improve the performance of open-winding permanent magnet synchronous motors (OW-PMSMs) with a common dc bus, a novel control method that can simultaneously eliminate parameter mismatch in the *d*-axis, *q*-axis, and zero-sequence loop (ZSL) is proposed. First, the parameter mismatches are analyzed. Second, an extended state observer (ESO), which can predict the current in the next instant and the disturbance caused by parameter mismatch, is established. By combining the ESO and the deadbeat predictive current control (DPCC) in the *d*-axis and *q*-axis, replacing the sampled current in the DPCC with the predictive current in the ESO, and considering predictive disturbance as a voltage reference feedforward compensation, one-step delay and the disturbance caused by parameter mismatch are addressed. Then, in the ZSL, the predicted zero-sequence disturbance is considered as a compensation for the reference zero-sequence voltage (ZSV). The ZSV is obtained using the zero-voltage vector redistribution strategy in alternate subhexagonal center pulsewidth modulation strategy. The proposed method enhances the robustness of OW-PMSM, against parameter mismatch in the *d*-axis, *q*-axis, or ZSL. To verify the effectiveness of the proposed method, simulation and experimental results obtained using the traditional DPCC method and the ESO+DPCC method are presented herein.**

***Index Terms*—Disturbance observer, extended state observer (ESO) open-winding permanent magnet synchronous motors (OW-PMSM), parameter mismatch, robustness.**

I. Introduction

RECENTLY, permanent magnet synchronous motor (PMSM) has been widely applied into industrial fields because of its many advantages such as high power density and good reliability [1]. However, a flux-weakening control method needs to be implemented when a higher speed is required with limited dc voltage, which could cause significant energy loss and even permanent demagnetization.

To solve this problem, the open-winding topology of PMSM (OW-PMSM), which opens the neutral point of stator windings and connects with another inverter [2], is proposed. The OW-PMSM enjoys many other advantages such as good fault tolerance and a multilevel modulation effect [3], [4], making it gain increasing attention.

A. Literature Review

Based on the difference in the power supply modes, OW-PMSM systems can be classified into two types, namely, systems with a common dc bus [5] and systems with an isolated dc bus [6]. Compared with systems having an isolated dc bus, systems having a common dc bus require smaller space and has less weight, which make them more attractive for various applications [7]. However, systems with a common dc bus have an inherent zero-sequence loop (ZSL). The zero-sequence current (ZSC) in ZSL adversely affects machine performance, and therefor needs to be suppressed [8]. There exist several control methods for OW-PMSM, such as field-oriented control [9] and direct torque control [10]. With the development of microprocessors over the last decades, many advanced control strategies, such as sliding-mode control [11] and model predictive control (MPC) [12], [13], have been implemented in power converters and drives. MPC uses a discrete model of the system, which has a good steady state and dynamic performance [14].

The two most common strategies of MPC are finite set control MPC (FSC-MPC) and continuous set control MPC (CSC-MPC) [15]–[17]. In FSC-MPC, the control action is defined by minimizing a cost function, which represents the desired behavior of the system; however, this leads to a large computational burden [15]. A long prediction horizon could improve the performance of the system compared with a short prediction horizon. However, the computational burden increases exponentially while needing long prediction horizon [17]. Many papers focused on computationally efficient optimization algorithms to reduce the computation complexity [18], [19]. In CSC-MPC, pulsewidth

Manuscript received January 14, 2020; revised June 21, 2020 and August 1, 2020; accepted September 8, 2020. Date of publication September 15, 2020; date of current version November 20, 2020. This work was supported in part by the key Areas of Guangdong Province under the project Integration and Industrialization of High Performance, Long Endurance and Integrated Electric Drive System, under Grant 2019B090910001 and in part by the Key Laboratory of Advanced Perception and Intelligent Control of High-end Equipment, Ministry of Education Open topic under Grant GDSC202008. Recommended for publication by Associate Editor J. Rodriguez. *(Corresponding author: Shuo Zhang.)*

The authors are with the Collaborative Innovation Center of Electric Vehicles in Beijing, School of Mechanical Engineering, Beijing Institute of Technology, Beijing 100081, China (e-mail: lixueping6677@163.com; shuozhangxd@163.com; mrzhchn@bit.edu.cn; zhouying6369@163.com; linshuchuntao@163.com).

Color versions of one or more of the figures in this article are available online at https://ieeexplore.ieee.org.

Digital Object Identifier 10.1109/TPEL.2020.3024227

modulation (PWM) is used to translate the desired voltages into switching orders; this results in a substantially lower computational burden compared with FSC-MPCC [20]. Meanwhile, it produces a fixed switching frequency, which could reduce the effects of resonance problems [21]. DPCC, which is used as a CCS-MPC method, forces the actual current of motor to track the reference current and achieves satisfactory steady state and dynamic state performance; hence, it has become one of the most applied control strategies in papers published in recent years. However, the MPC method relies on accurate machines model, which has high requirements for the exact OW-PMSM parameters, such as inductance, resistance and permanent magnet flux in the *d*-axis, *q*-axis, and ZSL [22]. The performance will deteriorate when parameter mismatch occurs. Moreover, parameter mismatch is inevitable when environment condition such as temperature changes [23]. Furthermore, control delay exists in DPCC, such as one-step delay in voltage calculation, can also deteriorate the performance of machines [24].

To solve the existing problems with DPCC, several methods have been studied. In [25], by adding an additional discrete-time current predictive unit to DPCC, the PMSM achieves a high performance while suffering from parametric uncertainties. While it has many similarities to the conventional PI control system, the gain parameters may be difficult to choose. In [26]–[29], the DPCC method was combined with a disturbance observer to enhance the robustness of the control system. An extended state observer (ESO) was presented in [26]. In that study, flux and inductance uncertainty were considered, but resistance mismatch, which has a noticeable effect on the performance of the control system, was overlooked. In [27], a Luenberger disturbance observer was designed to reduce the sensitivity of the control system to the aforementioned parameters. Meanwhile, it can increase the accuracy of speed. In [28], a simple adaptive disturbance observer was used to improve the performance of the control system under parameter mismatch, and torque ripple was suppressed as well. However, the systems in [27] and [28] still had a one-step delay, and the control system could not compensate for the disturbance in time. In [29], a disturbance observer based on the sliding-mode exponential reaching law was established, which can not only overcome the problem caused by parameter mismatch in the *d*-axis and *q*-axis, but also address the one-step delay problem. However, the structure of the observer is complex, which increases the burden of the control system.

The aforementioned methods are related to PMSM control system. In contrast, OW-PMSM with a common dc bus has an inherent ZSL. The ZSC in ZSL negatively affects the performance of an OW-PMSM control system; hence, it needs to be suppressed effectively. To reduce the frequency of switching, Somasekhar *et al.* [30] proposed an alternate subhexagonal center PWM modulation strategy (ASHCPWM). Based on ASHCPWM, a zero-voltage vector redistribution strategy was studied in [31], which could suppress the ZSC in stable state without requiring any additional element. However, Zhou and Nian [31] overlooked the ZSC in the dynamic state. Furthermore, ZSL parameter mismatch could result in unsatisfactory performance of the ZSC, which would lead to poor control performance of the OW-PMSM; Therefore, this should also be addressed. However, adequate research has not been conducted in this regard.

B. Motivation and Innovation

In order to enhance the robustness of an OW-PMSM control system, the parameter mismatches occurring in the *d*-axis, *q*-axis and ZSL should be considered simultaneously. This article proposes an improved method, termed ESO+DPCC control, which combines traditional DPCC, zero-voltage vector redistribution strategy in alternate subhexagonal center PWM modulation strategy (ZVRE-ASHCPWM), and an ESO. The most significant contribution of this article is that the proposed method can simultaneously eliminate the *d*-axis, *q*-axis, and ZSL parameter mismatch and one-step delay, unlike any existing method. The main contributions can be summarized as follows.

1) An ESO based on the *d*-axis and *q*-axis is established; it can predict disturbance caused by parameter mismatch in the *d*-axis and *q*-axis. The disturbance is regarded as the (k+1)th instant voltage reference feedforward compensation to improve the performance of OW-PMSM when parameter mismatch occurs in the *d*-axis and *q*-axis.
2) An ESO based on ZSL is established; it can predict the disturbance caused by zero-sequence loop parameter mismatch. The disturbance is regarded as the (k+1)th instant ZSV compensation to improve the performance of OW-PMSM when ZSL parameter mismatch occurs. ZSV is obtained using ZVRE-ASHCPWM.
3) ESO can predict the (k+1)th instant current in the *d*-axis, *q*-axis, and ZSL. The predicted current replaces the sampled current in DPCC. Moreover, in this process, the disturbance in the *d*-axis, *q*-axis, and ZSL can also be considered as a compensation to address one-step delay.
4) To verify the effectiveness of the proposed method, several simulation and experiments were conducted under different conditions.

The rest of this article is organized as follows. In Section II, the topology and mathematic model of OW-PMSM with a common dc bus is presented; then, DPCC and ASHPWM are introduced. In Section III, the parameter mismatch is analyzed, and the ESO is established. The stability of the ESO is analyzed, and subsequently, the proposed control method (ESO+DPCC) is illustrated. Sections IV and V show the results of the simulation and experiments. Finally, the conclusion is given in Section VI.

II. OW-PMSM With Common DC Bus

The topology of the OW-PMSM system with common dc bus is presented in Section II-A. The mathematical model of OW-PMSM is described in Section II-B, and the principle of DPCC is introduced in Section II-C. Section II-D presents the ASHPWM diagram and illustrates zero voltage vector distribution method (ZVRE-ASHCPWM).

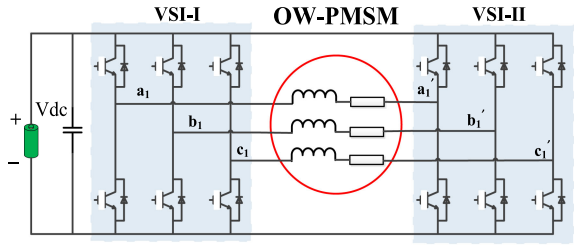

Fig. 1. Topology of OW-PMSM with common dc bus.

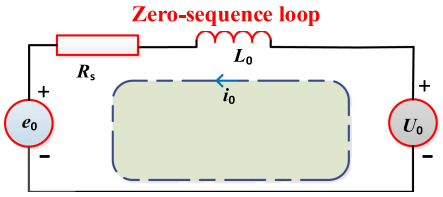

Fig. 2. Zero-sequence loop of OW-PMSMs.

A. Topology of OW-PMSM System With Common DC Bus

Fig. 1 shows the topology of OW-PMSM system with a common dc bus. Unlike in conventional PMSM, the neutral point is open, and there are two voltage-source inverter (VSI) systems. Compared with the isolated dc bus topology, the common dc bus topology needs smaller space and is lighter. However, it also leads to an inherent ZSL, as shown in Fig. 2.

B. Mathematical Model of OW-PMSM

Considering the ZSL, the mathematical model of OW-PMSM can be described as follows:

$$\begin{cases} U_{\mathrm{d}} = R_{\mathrm{s}} i_{\mathrm{d}} + L_{\mathrm{d}} \frac{di_{\mathrm{d}}}{dt} - \omega_{\mathrm{r}} L_{\mathrm{q}} i_{\mathrm{q}} \\ U_{\mathrm{q}} = R_{\mathrm{s}} i_{\mathrm{q}} + L_{\mathrm{q}} \frac{di_{\mathrm{q}}}{dt} + \omega_{\mathrm{r}} L_{\mathrm{d}} i_{\mathrm{d}} + \omega_{\mathrm{r}} \psi_{\mathrm{f}} \\ U_0 = R_{\mathrm{s}} i_0 + L_0 \frac{di_0}{dt} - 3\omega_{\mathrm{r}} \psi_{3\mathrm{f}} \sin(3\theta) \end{cases} \tag{1}$$

$$\begin{cases} U_0 = \frac{1}{3}(U_{\mathrm{a}} + U_{\mathrm{b}} + U_{\mathrm{c}}) \\ i_0 = \frac{1}{3}(i_{\mathrm{a}} + i_{\mathrm{b}} + i_{\mathrm{c}}) \end{cases} \tag{2}$$

$$T_{\mathrm{e}} = 1.5p * (\psi_{\mathrm{f}} i_{\mathrm{q}} + (L_{\mathrm{d}} - L_{\mathrm{q}}) i_{\mathrm{d}} i_{\mathrm{q}} - 6\psi_{3\mathrm{f}} \sin(3\theta) i_0) \tag{3}$$

where, U_{d}, U_{q}, and U_0 represent the d-axis voltage, q-axis voltage, and ZSL voltage, respectively; i_{d}, i_{q}, and i_0 represent the d-axis current, q-axis current, and zero-sequence current, respectively; R_{s}, L_{d}, L_{q}, L_0, Ψ_{f}, $\Psi_{3\mathrm{f}}$, θ, and ω_{r}, denote the winding resistance, d-axis inductance, q-axis inductance, ZSL inductance, fundamental flux-linkage, third-harmonic flux-linkage, electrical rotor position, and electrical angular speed, respectively; and U_{a}, U_{b}, U_{c}, i_{a}, i_{b}, and i_{c} are the voltages and currents of the a, b, and c phases, respectively. In OW-SPMSM, $L_{\mathrm{d}} = L_{\mathrm{q}} = L_{\mathrm{s}}$.

C. Principle of DPCC

DPCC can be divided into two parts: the prediction of the currents and the calculation of the voltages.

First, the mathematical model of OW-PMSM is discretized. If the sampling time T_{s} is sufficiently short, overlooking the ZSL,

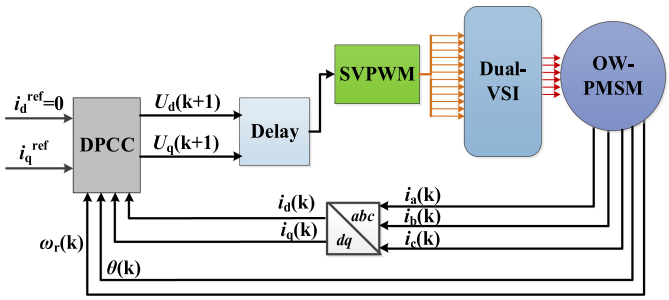

Fig. 3. Diagram of the principle of DPCC.

$i_{\mathrm{d}}(\mathrm{k+1})$ and $i_{\mathrm{q}}(\mathrm{k+1})$ can be estimated using

$$\begin{aligned} \hat{i}_{\mathrm{d}}(\mathrm{k+1}) &= \left(1 - \frac{R_{\mathrm{s}}}{L_{\mathrm{s}}} T_{\mathrm{s}}\right) i_{\mathrm{d}}(\mathrm{k}) + T_{\mathrm{s}} \omega_{\mathrm{r}}(\mathrm{k})\, i_{\mathrm{q}}(\mathrm{k}) + \frac{T_{\mathrm{s}}}{L_{\mathrm{s}}} U_{\mathrm{d}}(\mathrm{k}) \\ \hat{i}_{\mathrm{q}}(\mathrm{k+1}) &= \left(1 - \frac{R_{\mathrm{s}}}{L_{\mathrm{s}}} T_{\mathrm{s}}\right) i_{\mathrm{q}}(\mathrm{k}) - T_{\mathrm{s}} \omega_{\mathrm{r}}(\mathrm{k}) i_{\mathrm{d}}(\mathrm{k}) + \frac{T_{\mathrm{s}}}{L_{\mathrm{s}}} U_{\mathrm{q}}(\mathrm{k}) \\ &\quad - \frac{T_s}{L_s} \omega_{\mathrm{r}}(\mathrm{k})\, \psi_{\mathrm{f}} \end{aligned} \tag{4}$$

where $\hat{i}_d(\mathrm{k+1})$ and $\hat{i}_q(\mathrm{k+1})$ represent the estimation of the (k+1)th instant d-axis current and q-axis current, respectively. The (k+2)th instant current can be estimated using $\hat{i}_d(\mathrm{k+1})$ and $\hat{i}_q(\mathrm{k+1})$. We assume that $\omega_{\mathrm{r}}(\mathrm{k}) \approx \omega_{\mathrm{r}}(\mathrm{k+1})$ and $\theta(\mathrm{k}) \approx \theta(\mathrm{k+1})$. To allow the actual currents of the motor to track the current references after a modulation period, $\hat{i}_{\mathrm{s}}(\mathrm{k+2}) = i_{\mathrm{s}}{}^{\mathrm{ref}}(\mathrm{k})$, the (k+1)th instant voltage references can be described, as shown in (5). Since $\hat{i}_d(\mathrm{k+1})$ and $\hat{i}_q(\mathrm{k+1})$ are estimated, there is only one-step delay in the control system. The voltage references are obtained in the next SVPWM modulation period. The diagram of the principle of DPCC is shown in Fig. 3

$$\begin{aligned} U_{\mathrm{d}}(\mathrm{k+1}) &= \frac{L_{\mathrm{s}}}{T_{\mathrm{s}}} \Bigg(i_{\mathrm{d}}{}^{\mathrm{ref}}(\mathrm{k}) + \frac{R_{\mathrm{s}}}{L_{\mathrm{s}}} T_{\mathrm{s}} \hat{i}_{\mathrm{d}}(\mathrm{k+1}) \\ &\quad - T_{\mathrm{s}} \omega_{\mathrm{r}}(\mathrm{k}) \hat{i}_{\mathrm{q}}(\mathrm{k+1}) - \hat{i}_{\mathrm{d}}(\mathrm{k+1}) \Bigg) \\ U_q(\mathrm{k+1}) &= \frac{L_{\mathrm{s}}}{T_{\mathrm{s}}} \Bigg(i_{\mathrm{q}}{}^{\mathrm{ref}}(\mathrm{k}) + \frac{R_{\mathrm{s}}}{L_{\mathrm{s}}} T_{\mathrm{s}} \hat{i}_{\mathrm{q}}(\mathrm{k+1}) \\ &\quad + T_{\mathrm{s}} \omega_{\mathrm{r}}(\mathrm{k}) \hat{i}_{\mathrm{d}}(\mathrm{k+1}) + \frac{T_{\mathrm{s}}}{L_{\mathrm{s}}} \omega_{\mathrm{r}}(\mathrm{k})\, \psi_{\mathrm{f}} - \hat{i}_{\mathrm{q}}(\mathrm{k+1}) \Bigg). \end{aligned} \tag{5}$$

D. Alternate Subhexagonal Center PWM Modulation Diagram

As shown in Fig. 1, there are two inverters in the system. The desired voltage is generated by both the systems. Because of the high voltage vector utilization and low switching loss, ASHCPWM diagram (see Fig. 4) is often used to obtain the voltage vector.

U_{ref} denotes the voltage reference in the $\alpha\beta$ stationary frame. $U_{1\mathrm{ref}}$ and $U_{2\mathrm{ref}}$ denote the voltage references that VSI-1 and VSI-2, respectively, are required to produce. It can be seen that the entire hexagon is divided into six sectors, namely I, II, III, IV, V, and VI. When U_{ref} is located in I, III, or V, $U_{1\mathrm{ref}}$ is generated through a fixed switching state in VSI-1, and $U_{2\mathrm{ref}}$ is

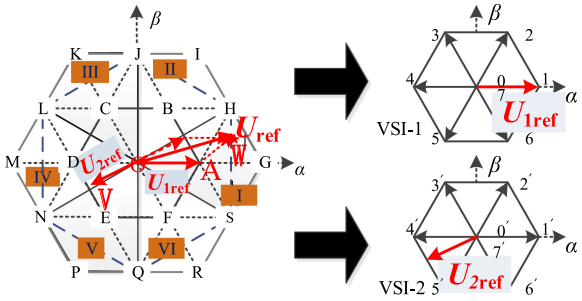

Fig. 4. Alternate subhexagonal center PWM modulation diagram.

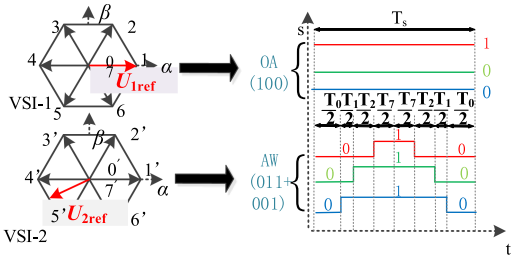

Fig. 5. Redistribution of the zero-voltage vector.

synthesized using the SVPWM technique in VSI-2. When U_{ref} is located in II, IV, or VI, $U_{2\mathrm{ref}}$ is generated through a fixed switching state in the VSI-2, and $U_{1\mathrm{ref}}$ is synthesized using the SVPWM technique in VSI-1.

For example, **OW** denotes the U_{ref} in Fig. 4, **OA** denotes $U_{1\mathrm{ref}}$ and **OV** denotes $U_{2\mathrm{ref}}$; **OW** = **OA**+**AW** = **OA-OV**. $U_{1\mathrm{ref}}$ is generated through a fixed switching state (100) in VSI-1, and, $U_{2\mathrm{ref}}$ is synthesized using SVPWM in VSI-2. In VSI-2, $U_{2\mathrm{ref}}$ is synthesized using sector 4'(011) and sector 5'(001). It is assumed that the durations of 4'(011) and 5'(001) are T_1 and T_2, respectively. In traditional SVPWM, the durations of 0' (000) T_0 and 7' (111) T_7 are equal, as shown in

$$T_0 = T_7 = \frac{1}{2}\left(T_{\mathrm{s}} - T_1 - T_2\right). \tag{6}$$

$U_{1\mathrm{ref}}$ and $U_{2\mathrm{ref}}$ are shown in (7), where V_{dc} denotes the dc voltage in the system, and $U_{1\mathrm{ref}\alpha}$, $U_{1\mathrm{ef}\beta}$, $U_{2\mathrm{ref}\alpha}$, and $U_{2\mathrm{ef}\beta}$ denote, respectively, the desired voltages that VSI-1 and VSI-2 need to produce in the $\alpha\beta$ stationary frame

$$\begin{cases}
\text{sector I} \begin{cases} U_{1\mathrm{ref}\alpha} = \frac{2}{3}V_{\mathrm{dc}}, U_{1\mathrm{ref}\beta} = 0 \\ U_{2\mathrm{ref}\alpha} = -\left(U_{\mathrm{ref}\alpha} - \frac{2}{3}V_{\mathrm{dc}}\right), U_{2\mathrm{ref}\beta} = -U_{\mathrm{ref}\beta} \end{cases} \\
\text{sector II} \begin{cases} U_{1\mathrm{ref}\alpha} = U_{\mathrm{ref}\alpha} - \frac{1}{3}V_{\mathrm{dc}}, \\ U_{1\mathrm{ref}\beta} = U_{\mathrm{ref}\beta} - \frac{\sqrt{3}}{3}V_{\mathrm{dc}} \\ U_{2\mathrm{ref}\alpha} = -\frac{1}{3}V_{\mathrm{dc}}, U_{2\mathrm{ref}\beta} = -\frac{\sqrt{3}}{3}V_{\mathrm{dc}} \end{cases} \\
\text{sector III} \begin{cases} U_{1\mathrm{ref}\alpha} = -\frac{1}{3}V_{\mathrm{dc}}, U_{1\mathrm{ref}\beta} = -\frac{\sqrt{3}}{3}V_{\mathrm{dc}} \\ U_{2\mathrm{ref}\alpha} = -\left(U_{\mathrm{ref}\alpha} + \frac{1}{3}V_{\mathrm{dc}}\right) \\ U_{2\mathrm{ref}\beta} = -\left(U_{\mathrm{ref}\beta} + \frac{\sqrt{3}}{3}V_{\mathrm{dc}}\right) \end{cases} \\
\text{sector IV} \begin{cases} U_{1\mathrm{ref}\alpha} = U_{\mathrm{ref}\alpha} + \frac{2}{3}V_{\mathrm{dc}}, U_{1\mathrm{ref}\beta} = U_{\mathrm{ref}\beta} \\ U_{2\mathrm{ref}\alpha} = -\frac{2}{3}V_{\mathrm{dc}}, U_{2\mathrm{ref}\beta} = 0 \end{cases} \\
\text{sector V} \begin{cases} U_{1\mathrm{ref}\alpha} = -\frac{1}{3}V_{\mathrm{dc}}, U_{1\mathrm{ref}\beta} = -\frac{\sqrt{3}}{3}V_{\mathrm{dc}} \\ U_{2\mathrm{ref}\alpha} = -\left(U_{\mathrm{ref}\alpha} + \frac{2}{3}V_{\mathrm{dc}}\right) \\ U_{2\mathrm{ref}\beta} = -\left(U_{\mathrm{ref}\beta} + \frac{\sqrt{3}}{3}V_{\mathrm{dc}}\right) \end{cases} \\
\text{sector VI} \begin{cases} U_{1\mathrm{ref}\alpha} = U_{\mathrm{ref}\alpha} + \frac{1}{3}V_{\mathrm{dc}}, \\ U_{1\mathrm{ref}\beta} = U_{\mathrm{ref}\beta} + \frac{\sqrt{3}}{3}V_{\mathrm{dc}} \\ U_{2\mathrm{ref}\alpha} = -\frac{1}{3}V_{\mathrm{dc}}, U_{2\mathrm{ref}\beta} = \frac{\sqrt{3}}{3}V_{\mathrm{dc}}. \end{cases}
\end{cases} \tag{7}$$

However, to ensure that the motor has a stable performance, the ZSC needs to be suppressed. In [32], the redistribution concept is to counteract the third back EMF that overlooks the dynamic response. In this article, according to the principle of DPCC, we can predict the (k+1)th instant ZSC $\hat{i}_0$(k+1) and calculate the voltage U_0(k+1), as shown in (8) and (9), respectively, which consider both the static and dynamic responses

$$\hat{i}_0\left(\mathrm{k}+1\right) = \left(1 - \frac{R_{\mathrm{s}}}{L_0}T_{\mathrm{s}}\right) i_0\left(\mathrm{k}\right) + 3\frac{T_{\mathrm{s}}}{L_0}\psi_{3\mathrm{f}}\omega_{\mathrm{r}}\left(\mathrm{k}\right)\sin\left(3\theta\left(\mathrm{k}\right)\right) + \frac{T_{\mathrm{s}}}{L_0}U_0\left(\mathrm{k}\right) \tag{8}$$

$$U_0\left(\mathrm{k}+1\right) = \frac{L_0}{T_{\mathrm{s}}}\left(i_0{}^{\mathrm{ref}}\left(\mathrm{k}\right) + \frac{R_{\mathrm{s}}}{L_0}T_{\mathrm{s}}\hat{i}_0\left(\mathrm{k}+1\right) - \hat{i}_0\left(\mathrm{k}+1\right)\right) - 3\omega_{\mathrm{r}}\left(\mathrm{k}\right)\psi_{3\mathrm{f}}\sin\left(3\theta\left(\mathrm{k}\right)\right). \tag{9}$$

To suppress the ZSC, the dwell time of the zero-voltage vector needs to be redistributed to generate the required voltage U_0(k+1). The total time of the zero-voltage vector is T_{zero}

$$T_{\mathrm{zero}} = T_0 + T_7 = T_{\mathrm{s}} - T_1 - T_2. \tag{10}$$

The distribution factor of the zero-voltage sector x_{zero} should be recalculated

$$\begin{cases} T_0 = \frac{T_{\mathrm{zero}}x_{\mathrm{zero}}}{2} \\ T_7 = \frac{2T_{\mathrm{zero}} - T_{\mathrm{zero}}x_{\mathrm{zero}}}{2}. \end{cases} \tag{11}$$

From Fig. 5, during sampling time Ts, the average value of ZSV

$$\overline{\mathrm{ZSV}} = \left(\frac{V_{\mathrm{dc}}}{3}T_{\mathrm{s}} - \frac{V_{\mathrm{dc}}}{3}T_1 - \frac{2V_{\mathrm{dc}}}{3}T_2 - V_{\mathrm{dc}}\frac{2T_{\mathrm{zero}} - T_{\mathrm{zero}}x_{\mathrm{zero}}}{2}\right)/T_{\mathrm{s}}. \tag{12}$$

To ensure that the ZSC is equal to zero

$$\overline{\mathrm{ZSV}} = U_0\left(\mathrm{k}+1\right). \tag{13}$$

From (11)–(13)

$$x_{\mathrm{zero}} = \frac{2U_0\left(\mathrm{k}+1\right)T_{\mathrm{s}}}{\mathrm{V_{dc}}T_{\mathrm{zero}}} - \frac{2T_{\mathrm{s}}}{3T_{\mathrm{zero}}} + \frac{2T_1}{3T_{\mathrm{zero}}} + \frac{4T_2}{3T_{\mathrm{zero}}} + 2. \tag{14}$$

In an actual situation, x_{zero} has a limit, $0 \leq x_{\mathrm{zero}} \leq 2$, because of which i_0 is not equal to zero in some cases. After obtaining x_{zero}, the durations of S_{a1}, S_{b1}, S_{c1}, S_{a2}, S_{b2}, and S_{c2} can be expressed as (15). Based on (15), U_{ref} is generated, and ZSC is

TABLE I
RIGHT TIME DURATION WHEN IN DIFFERENT SECTORS

Sector	1', 2'	2',3'	3', 4'	4',5'	5',6'	6',1'
S_{a2}	T_{c2on}	T_{b2on}	T_{a2on}	T_{a2on}	T_{b2on}	T_{b2on}
S_{b2}	T_{b2on}	T_{c2on}	T_{c2on}	T_{b2on}	T_{a2on}	T_{a2on}
S_{c2}	T_{a2on}	T_{a2on}	T_{b2on}	T_{c2on}	T_{c2on}	T_{c2on}

suppressed

$$\begin{cases} T_{\mathrm{a1on}} = T_{\mathrm{s}} \\ T_{\mathrm{b1on}} = 0 \\ T_{\mathrm{c1on}} = 0 \\ T_{\mathrm{a2on}} = \frac{2T_{\mathrm{zero}} - T_{\mathrm{zero}} x_{\mathrm{zero}}}{2} \\ T_{\mathrm{b2on}} = T_{\mathrm{a2on}} + T_2 \\ T_{\mathrm{c2on}} = T_{\mathrm{b2on}} + T_1. \end{cases} \tag{15}$$

Furthermore, when $U_{2\mathrm{ref}}$ is located in other sectors, the principle of SVPWM is the same as in (12)–(16). The time durations of $S_{\mathrm{a}2}$, $S_{\mathrm{b}2}$, and $S_{\mathrm{c}2}$ are presented in Table I.

III. EXTENDED STATE OBSERVER CONTROL BASED ON DEADBEAT PREDICTIVE CURRENT CONTROL (ESO+DPCC)

From (1), (4), and (5), it follows that the conventional DPCC method is based on the accurate parameters of a motor, such as L_{d}, L_{q}, R_{s}, L_0, Ψ_{f}, and $\Psi_{3\mathrm{f}}$. However, these parameters inevitably change during the operation of the motor [23]. To solve this problem, this article presents an improved predictive current control method. Section III-A analyzes the effects of parameter inaccuracy. ESO is established, and its stability is analyzed in Sections III-B and III-C. A novel control method, termed extended state observer control based on deadbeat predictive current control and ZVRE-ASHCPWM (ESO+DPCC), is proposed in Section III-D.

A. Parameter Inaccuracy Analysis

Inaccurate parameters of the motor could cause voltage references inaccuracy, which degrades the control performance [23]. According to [29], and considering the ZSL, if the true parameters of a motor are R_s', L_s', Ψ_{f}', L_0', and $\Psi_{3\mathrm{f}}'$, (1) can be written as

$$\begin{cases} U_{\mathrm{d}} = R_{\mathrm{s}} i_{\mathrm{d}} + L_{\mathrm{s}} \frac{di_{\mathrm{d}}}{dt} - \omega_{\mathrm{r}} L_{\mathrm{s}} i_{\mathrm{q}} + f_{\mathrm{d}} \\ U_{\mathrm{q}} = R_{\mathrm{s}} i_{\mathrm{q}} + L_{\mathrm{s}} \frac{di_{\mathrm{q}}}{dt} + \omega_{\mathrm{r}} L_{\mathrm{s}} i_{\mathrm{d}} + \omega_{\mathrm{r}} \varphi_{\mathrm{f}} + f_{\mathrm{q}} \\ U_0 = R_{\mathrm{s}} i_0 + L_0 \frac{di_0}{dt} - 3\omega_{\mathrm{r}} \varphi_{3\mathrm{f}} \sin(3\theta) + f_0 \end{cases} \tag{16}$$

$$\begin{aligned} f_{\mathrm{d}} &= \Delta R_{\mathrm{s}} i_{\mathrm{d}} + \Delta L_{\mathrm{s}} \frac{di_{\mathrm{d}}}{dt} - \omega_{\mathrm{r}} \Delta L_{\mathrm{s}} i_{\mathrm{q}} \\ f_{\mathrm{q}} &= \Delta R_{\mathrm{s}} i_{\mathrm{q}} + \Delta L_{\mathrm{s}} \frac{di_{\mathrm{q}}}{dt} + \omega_{\mathrm{r}} \Delta L_{\mathrm{s}} i_{\mathrm{d}} + \omega_{\mathrm{r}} \Delta \varphi_{\mathrm{f}} \\ f_0 &= \Delta R_{\mathrm{s}} i_0 + \Delta L_0 \frac{di_0}{dt} - 3\omega_{\mathrm{r}} \Delta \psi_{3\mathrm{f}} \sin(3\theta) \end{aligned} \tag{17}$$

where $\Delta R = R_s' - R_s$, $\Delta L = L_s' - L_s$, $\Delta L_0 = L_0' - L_0$, $\Delta\Psi_{3\mathrm{f}} = \Psi_{3\mathrm{f}}' - \Psi_{3\mathrm{f}}$, and $\Delta\Psi_{\mathrm{f}} = \Psi_{\mathrm{f}}' - \Psi_{\mathrm{f}}$. Also, f_{d}, f_{q}, and f_0 are the disturbances caused by parameter inaccuracy, which have a significant effect on the control performance but cannot be measured directly. Therefore, $f_{\mathrm{d}}, f_{\mathrm{q}}, f_0$ should be estimated accurately. Equation (16) can be written as

$$U_{\mathrm{d}} = R_{\mathrm{s}} \hat{i}_{\mathrm{d}} + L_s \frac{d\hat{i}_{\mathrm{d}}}{dt} - \omega_{\mathrm{r}} L_{\mathrm{s}} i_{\mathrm{q}} + \hat{f}_{\mathrm{d}}$$

$$U_{\mathrm{q}} = R_{\mathrm{s}} \hat{i}_{\mathrm{q}} + L_s \frac{d\hat{i}_{\mathrm{q}}}{dt} + \omega_{\mathrm{r}} L_{\mathrm{s}} i_{\mathrm{d}} + \omega_{\mathrm{r}} \varphi_{\mathrm{f}} + \hat{f}_{\mathrm{q}}$$

$$U_0 = R_{\mathrm{s}} \hat{i}_0 + L_0 \frac{d\hat{i}_0}{dt} - 3\omega_{\mathrm{r}} \varphi_{3\mathrm{f}} \sin(3\theta) + \hat{f}_0 \tag{18}$$

where $\hat{f}_d$, $\hat{f}_q$,and $\hat{f}_0$ are the estimations of $f_{\mathrm{d}}, f_{\mathrm{q}}$, and f_0, respectively.

B. Establishment of ESO

ESO can estimate the state variables that are unknown depending on some known state variables [32]. In this article, f_{d}, f_{q}, and f_0 are regarded as unknown state variables, which must be estimated accurately. The principle of ESO is as follows:

$$\begin{aligned} \dot{x}_1 &= A_1 x_1 + A_2 x_2 - \gamma_1 E_1 + bU \\ \dot{x}_2 &= -\gamma_2 |E_1|^{\alpha_1} \mathrm{sat}\left(\frac{E_1}{\xi_1}\right) \end{aligned} \tag{19}$$

where x_1 denotes the state variables that can be measured and estimated, and x_2 denotes the state variables that cannot be measured and should be estimated. A_1, A_2, and b are matrices related to the control system, $E_1 = {}^x1$ -x_1. γ_1, α_1, ξ_1, and γ_2 are parameters of the ESO. *Sat(X)* is defined as follows:

$$\mathrm{sat}(X) = \begin{cases} X & |X| <= 1 \\ \mathrm{sign}(X) & |X| > 1 \end{cases}. \tag{20}$$

ESO and OW-PMSM are combined

$$\begin{cases} \frac{d\hat{i}_{\mathrm{d}}}{dt} = -\frac{R_{\mathrm{s}}}{L_{\mathrm{s}}} \hat{i}_{\mathrm{d}} + \omega_{\mathrm{r}} i_{\mathrm{q}} + \frac{1}{L_{\mathrm{s}}} U_{\mathrm{d}} - \frac{1}{L_{\mathrm{s}}} \hat{f}_{\mathrm{d}} - \gamma_1 \mathrm{e}_1 \\ \frac{d\hat{f}_{\mathrm{d}}}{dt} = -\gamma_2 |e_1|^{\alpha_1} \mathrm{sat}\left(\frac{e_1}{\xi_1}\right) \end{cases} \tag{21}$$

$$\begin{cases} \frac{d\hat{i}_{\mathrm{q}}}{dt} = -\frac{R_{\mathrm{s}}}{L_{\mathrm{s}}} \hat{i}_{\mathrm{q}} - \omega_{\mathrm{r}} i_{\mathrm{d}} - \frac{1}{L_{\mathrm{s}}} \omega_{\mathrm{r}} \varphi_{\mathrm{f}} + \frac{1}{L_{\mathrm{s}}} U_{\mathrm{q}} - \frac{1}{L_{\mathrm{s}}} \hat{f}_{\mathrm{q}} - \gamma_3 \mathrm{e}_2 \\ \frac{d\hat{f}_{\mathrm{q}}}{dt} = -\gamma_4 |e_2|^{\alpha_2} \mathrm{sat}\left(\frac{e_2}{\xi_2}\right) \end{cases} \tag{22}$$

$$\begin{cases} \frac{d\hat{i}_0}{dt} = -\frac{R_{\mathrm{s}}}{L_0} \hat{i}_0 + \frac{1}{L_0} 3\omega_{\mathrm{r}} \varphi_{3\mathrm{f}} \sin(3\theta) + \frac{1}{L_0} U_0 - \frac{1}{L_0} \hat{f}_0 - \gamma_5 \mathrm{e}_3 \\ \frac{d\hat{f}_0}{dt} = -\gamma_6 |e_3|^{\alpha_3} \mathrm{sat}\left(\frac{e_3}{\xi_3}\right) \end{cases} \tag{23}$$

where γ_{i} (i = 1,2,3,4,5,6), and α_{i} (i = 1,2,3), ξ_{i} (i = 1,2,3) are the parameters of the ESO. γ_{i} should be selected to ensure the stability of the observer, $\alpha_{\mathrm{i}} = 0.5$ or 1 and $\xi_{\mathrm{i}} = 0.01$ usually. $e_1 = \hat{i}_d$ -i_{d}, $e_2 = \hat{i}_q$ -i_{q}, and $e_3 = \hat{i}_0$ -i_0.

Equations (21)–(23) are discretized and linearized

$$\begin{cases} \hat{i}_{\mathrm{d}}(\mathrm{k}+1) = \left(1 - \frac{R_{\mathrm{s}}}{L_{\mathrm{s}}} T_{\mathrm{s}}\right) \hat{i}_{\mathrm{d}}(\mathrm{k}) + T_{\mathrm{s}} \omega_{\mathrm{r}}(\mathrm{k})\, i_{\mathrm{q}}(\mathrm{k}) \\ + \frac{T_{\mathrm{s}}}{L_{\mathrm{s}}} U_{\mathrm{d}}(\mathrm{k}) - \frac{T_{\mathrm{s}}}{L_{\mathrm{s}}} \hat{f}_{\mathrm{d}}(\mathrm{k}) - \gamma_1 \mathrm{e}_1(\mathrm{k})\, T_{\mathrm{s}} \\ \hat{f}_d(\mathrm{k}+1) = \hat{f}_d(\mathrm{k}) + T_{\mathrm{s}} \left(-\gamma_2 |e_1|^{\alpha_1} \mathrm{sat}\left(\frac{e_1}{\xi_1}\right)\right) \end{cases} \tag{24}$$

$$\begin{cases} \hat{i}_{\mathrm{q}}(\mathrm{k}+1) = \left(1 - \frac{R_{\mathrm{s}}}{L_{\mathrm{s}}} T_{\mathrm{s}}\right) \hat{i}_{\mathrm{q}}(\mathrm{k}) - T_{\mathrm{s}} \omega_{\mathrm{r}}(\mathrm{k})\, i_{\mathrm{d}}(\mathrm{k}) + \frac{T_{\mathrm{s}}}{L_{\mathrm{s}}} U_{\mathrm{q}}(\mathrm{k}) \\ - \frac{T_{\mathrm{s}}}{L_{\mathrm{s}}} \omega_{\mathrm{r}}(\mathrm{k})\, \psi_{\mathrm{f}} - \frac{T_s}{L_s} \hat{f}_{\mathrm{q}}(\mathrm{k}) - \gamma_3 \mathrm{e}_2(\mathrm{k})\, T_{\mathrm{s}} \\ \hat{f}_{\mathrm{q}}(\mathrm{k}+1) = \hat{f}_{\mathrm{q}}(\mathrm{k}) + T_{\mathrm{s}} \left(-\gamma_4 |e_2|^{\alpha_2} \mathrm{sat}\left(\frac{e_2}{\xi_2}\right)\right) \end{cases} \tag{25}$$

$$\begin{cases} \hat{i}_0\left(\mathrm{k}+1\right)=\left(1-\frac{R_\mathrm{s}}{L_0}T_\mathrm{s}\right)\hat{i}_0\left(\mathrm{k}\right)+\frac{T_\mathrm{s}}{L_0}6\psi_{3\mathrm{f}}\omega_\mathrm{r}\left(\mathrm{k}\right)\sin\left(3\theta\left(\mathrm{k}\right)\right) \\ +\frac{T_\mathrm{s}}{L_0}U_0\left(\mathrm{k}\right)-\frac{T_\mathrm{s}}{L_0}\hat{f}_0\left(\mathrm{k}\right)-\gamma_5 e_3\left(\mathrm{k}\right)T_\mathrm{s} \\ \hat{f}_0\left(\mathrm{k}+1\right)=\hat{f}_0(\mathrm{k})+T_\mathrm{s}\left(-\gamma_6|e_3|^{\alpha_3}\mathrm{sat}\left(\frac{e_3}{\xi_3}\right)\right). \end{cases} \tag{26}$$

C. Stability Analysis of ESO

To ensure the convergence of e_1, e_2, and e_3, γ_i (i = 1,3,5) should be chosen appropriately. The Lyapunov function V can be written as shown in (27) and should satisfy (28) as follows:

$$V=\frac{1}{2}{e_1}^2 \tag{27}$$

$$\dot{V}=e_1\dot{e}_1\le 0. \tag{28}$$

From (16) and (21)

$$\begin{aligned}\dot{V}=e_1\dot{e}_1&=e_1\left(-\frac{R_\mathrm{s}}{L_\mathrm{s}}e_1-\gamma_1 e_1-\frac{1}{L_\mathrm{s}}\left(\hat{f}_\mathrm{d}-f_\mathrm{d}\right)\right)\\&=\begin{cases}0 & e_1=0\\ -\left(\frac{R_\mathrm{s}}{L_\mathrm{s}}+\gamma_1\right){e_1}^2-\frac{e_1}{L_\mathrm{s}}\left(\hat{f}_\mathrm{d}-f_\mathrm{d}\right) & e_1\ne 0\end{cases}.\end{aligned} \tag{29}$$

From (29), it should be ensured that (28) and the following equations are satisfied:

$$\frac{R_\mathrm{s}}{L_\mathrm{s}}+\gamma_1\ge 0\longrightarrow\gamma_1\le-\frac{R_\mathrm{s}}{L_\mathrm{s}} \tag{30}$$

$$e_1\left(\hat{f}_\mathrm{d}-f_\mathrm{d}\right)\ge 0. \tag{31}$$

Equation (31) is discretized and linearized

$$\hat{f}_\mathrm{d}\left(\mathrm{k}\right)=f_\mathrm{d}\left(0\right)-\gamma_2 T_\mathrm{s}\sum_{i=1}^{k}\left(|e_\mathrm{i}|^{\alpha_1}\mathrm{sat}\left(\frac{e_\mathrm{i}}{\xi_1}\right)\right). \tag{32}$$

Assuming that $f_\mathrm{d}(0)=0$ and $\hat{f}_d(\mathrm{k}\text{-}1)\approx f_\mathrm{d}(\mathrm{k}\text{-}1)$, $\hat{f}_\mathrm{d}(\mathrm{k})=\hat{f}_\mathrm{d}(\mathrm{k}-1)-\gamma_2 T_s(|e_1(\mathrm{k})|^{\alpha_1}\mathrm{sat}(\frac{e_1(\mathrm{k})}{\xi_1})$

$$\begin{aligned}&e_1\left(\mathrm{k}\right)\left(\hat{f}_\mathrm{d}\left(\mathrm{k}\right)-f_\mathrm{d}\left(\mathrm{k}\right)\right)\\&=e_1\left(\mathrm{k}\right)\left(-\gamma_2 T_\mathrm{s}\left(|e_1\left(\mathrm{k}\right)|^{\alpha_1}\right)sat\left(\frac{e_1(\mathrm{k})}{\xi_1}\right)-\Delta f_\mathrm{d}\left(\mathrm{k}\right)\right)\ge 0.\end{aligned} \tag{33}$$

We can get that

$$\gamma_2\le\frac{-\Delta f_\mathrm{d}\left(\mathrm{k}\right)}{T_\mathrm{s}\left(|e_1\left(\mathrm{k}\right)|^{\alpha_1}\right)\mathrm{sat}\left(\frac{e_1(\mathrm{k})}{\xi_1}\right)}. \tag{34}$$

Similarly

$$\begin{cases}\gamma_3\le\frac{R_\mathrm{s}}{L_\mathrm{s}}\\ \gamma_4\le\frac{-\Delta f_\mathrm{q}(\mathrm{k})}{T_\mathrm{s}\left(|e_2(\mathrm{k})|^{\alpha_2}\mathrm{sat}\left(\frac{e_2(\mathrm{k})}{\xi_2}\right)\right)}\\ \gamma_5\le\frac{R_\mathrm{s}}{L_0}\\ \gamma_6\le\frac{-\Delta f_0(\mathrm{k})}{T_s\left(|e_3(\mathrm{k})|^{\alpha_3}\mathrm{sat}\left(\frac{e_3(\mathrm{k})}{\xi_3}\right)\right)}.\end{cases} \tag{35}$$

where α_i and ξ_i can be set as 1 and 0.01, respectively. According to the analysis provided previously, by choosing a suitable γ_i, the observer can be proved to be stable.

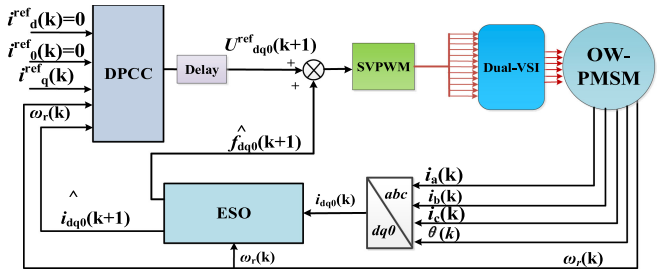

Fig. 6. Block diagram of ESO+DPCC.

D. ESO+DPCC Control Method

By applying ESO into OW-PMSM, f_d, f_q, and f_0 can be estimated. By replacing the traditional DPCC control method with the improved ESO+DPCC control method, (5) could be rewritten as (36). The ESO+DPCC control method can be expressed as a combination of (24)–(26) and

$$\begin{aligned}U_\mathrm{d}\left(\mathrm{k}+1\right)&=\frac{L_\mathrm{s}}{T_\mathrm{s}}\left(i_\mathrm{d}{}^{\mathrm{ref}}+\frac{R_\mathrm{s}}{L_\mathrm{s}}T_\mathrm{s}\hat{i}_\mathrm{d}\left(\mathrm{k}+1\right)-T_\mathrm{s}\omega_\mathrm{r}\left(\mathrm{k}\right)\hat{i}_\mathrm{q}\left(\mathrm{k}+1\right)\right.\\&\left.-\hat{i}_\mathrm{d}\left(\mathrm{k}+1\right)\right)+\hat{f}_\mathrm{d}\left(\mathrm{k}+1\right)\\U_\mathrm{q}\left(\mathrm{k}+1\right)&=\frac{L_\mathrm{s}}{T_\mathrm{s}}\left(i_\mathrm{q}{}^{\mathrm{ref}}+\frac{R_\mathrm{s}}{L_\mathrm{s}}T_\mathrm{s}\hat{i}_\mathrm{q}\left(\mathrm{k}+1\right)+T_\mathrm{s}\omega_\mathrm{r}\left(\mathrm{k}\right)\hat{i}_\mathrm{d}\left(\mathrm{k}+1\right)\right.\\&\left.+\frac{T_\mathrm{s}}{L_\mathrm{s}}w_\mathrm{r}\left(\mathrm{k}\right)\psi_\mathrm{f}-\hat{i}_\mathrm{q}\left(\mathrm{k}+1\right)\right)+\hat{f}_\mathrm{q}\left(\mathrm{k}+1\right)\\U_0\left(\mathrm{k}+1\right)&=\frac{L_0}{T_0}\left(i_0{}^{\mathrm{ref}}+\frac{R_\mathrm{s}}{L_0}T_\mathrm{s}\hat{i}_0\left(\mathrm{k}+1\right)-\hat{i}_0\left(\mathrm{k}+1\right)\right)\\&\left.-3\omega_\mathrm{r}\left(\mathrm{k}\right)\varphi_{3\mathrm{f}}\sin\left(3\theta\left(\mathrm{k}\right)\right)\right)+\hat{f}_0\left(\mathrm{k}+1\right).\end{aligned} \tag{36}$$

The diagram of ESO+DPCC is showed in Fig. 6.

It is observed that the disturbance caused by parameter mismatch can be estimated and regarded as a feedforward compensation for the voltage references; this can enhance the control performance of OW-PMSM.

IV. Simulation Study

To evaluate the effectiveness of the proposed method, the traditional DPCC control method (denoted as Method 1) and ESO+DPCC control method (denoted as Method 2) are implemented using MATLAB/Simulink. The parameters of OW-PMSM are presented in Table II. The control time is set to 50 μs, the simulation sample time is set to 5 μs, the dc voltage is set to 100 V. To ensure greater consistency with an actual situation, the deadtime is set to 2.5 μs. The parameters of ESO are $\gamma_1=\gamma_3=-12\,000$, $\gamma_5=-13\,000$; $\alpha_1=\alpha_2=\alpha_3=1$; $\xi_1=\xi_2=\xi_3=0.01$; and $\gamma_2=\gamma_4=-2000$, $\gamma_6=-4000$.

The performance of OW-PMSM without parameter mismatch ($R'_s=R_s$, $L'_s=L_s$, $L'_0=L_0$, $\Psi'_{3\mathrm{f}}=\Psi_{3\mathrm{f}}$, and $\Psi'_\mathrm{f}=\Psi_\mathrm{f}$) is shown in Fig. 7. The load torque ranges from 1 N·m to 4 N·m and then from 4 N·m to 2 N·m. Here, $i_{\mathrm{d\ ref}}$ and $i_{\mathrm{q\ ref}}$ represent the current references in d-axis and q-axis, respectively. In the

TABLE II
OW-PMSM PARAMETERS

Parameter	Description	Value
P	Number of pole pairs	4
R_S	Stator resistance (Ω)	1.38
L_S	Stator inductance (mH)	3.21
L_0	Zero-sequence inductance (mH)	3.1
Ψ_{3f}	Rotor third harmonic flux linkage (Wb)	0.008
I_N	Rated Current (A)	4
Ψ_f	Rotor flux linkage (Wb)	0.1667
T_N	Rated torque (Nm)	4
J	Rotational inertia (kg • m^2)	0.00085

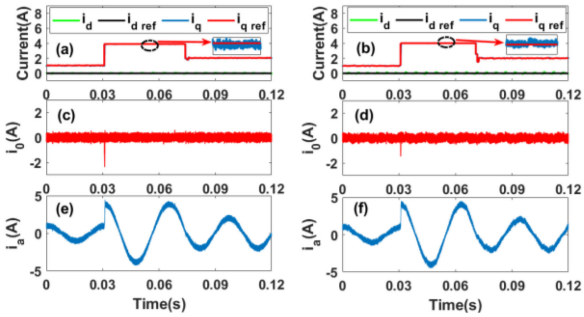

Fig. 7. Simulation results under no parameter mismatch condition. (a), (c), and (e) Method 1. (b), (d), and (f) Method 2.

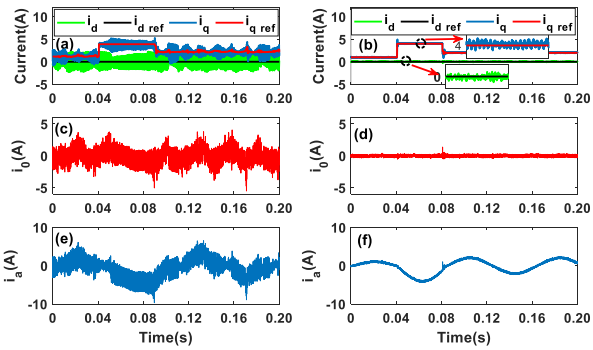

Fig. 8. Simulation results at 200 r/min under $L'_s = 2L_s$ condition. (a), (c), and (e) Method 1. (b), (d), and (f) Method 2.

absence of parameter mismatch, the two methods are almost identical. The currents i_d and i_q can track the current references (i_d reference and i_q reference, respectively). In addition, ZSC (i_0) exhibits satisfactory performance.

Second, to observe the effectiveness of the proposed control method, some parameter mismatch simulation results are shown in Figs. 8 –12. Fig. 8 presents the situation when $L'_s = 2L_s$. The performance of the traditional DPCC control method has more harmonic content. Fig. 9 shows the simulation results obtained using the two methods under zero-sequence loop inductance, $L'_0 = 2L_0$. The ZSC of Method 1 is larger than that of Method 2. This shows that the Method 2 can suppress the disturbances caused by ZSL inductance mismatch.

Fig. 10 shows the simulation results under $\Psi'_f = 1.5\Psi_f$ condition. Here, because i_0 and i_a exhibit nearly the same performance in both methods, we omit them. It can be seen that under this condition, i_q and i_q references always have a clear difference in

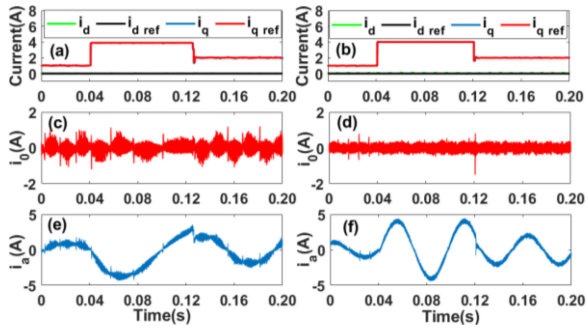

Fig. 9. Simulation results at 300 r/min under $L'_0 = 2L_0$ condition. (a), (c), and (e) Method 1. (b), (d), and (f) Method 2.

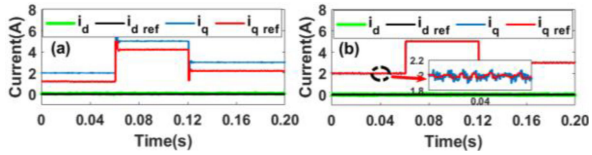

Fig. 10. Simulation results at 900 r/min under $\Psi'_f = 1.5\Psi_f$ condition. (a) Method 1. (b) Method 2.

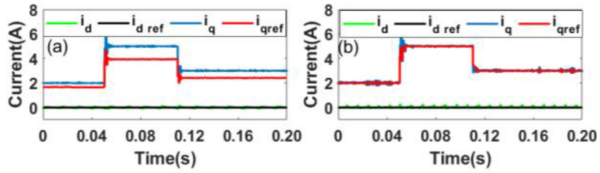

Fig. 11. Simulation results at 400 r/min under $R'_s = 7R_s$ condition. (a) Method 1. (b) Method 2.

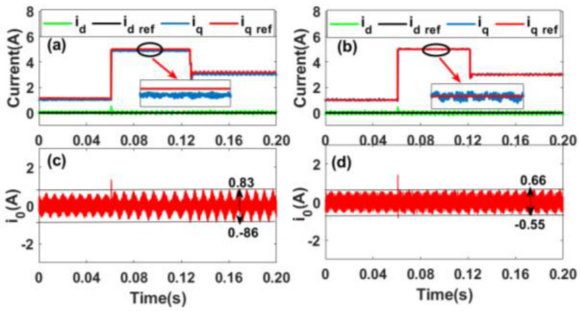

Fig. 12. Simulation results at 700 r/min under $\Psi'_{3f} = 0.25\Psi_{3f}$ condition. (a) and (c) Method 1. (b) and (d) Method 2.

Method 1. However, in Method 2, i_q can track the i_q reference accurately.

Moreover, the performance of the two methods under $R'_s = 7R_s$ and $\Psi'_{3f} = 0.25\Psi_{3f}$, shown in Figs. 11 and 12, respectively, is the same.

Fig. 13 shows a comparison between the two methods under a complex condition that $R'_s = 0.2R_s$, $L'_s = 2L_s$, $L'_0 = 2L_0$, $\Psi'_{3f} = 0.25\Psi_{3f}$, and $\Psi'_f = 0.5\Psi_f$. The performance of Method 2 is better than that of Method 1. This shows that the Method 2 can suppress complex parameter mismatch disturbances. Therefore, it can be concluded that Method 2 is more robust under different conditions.

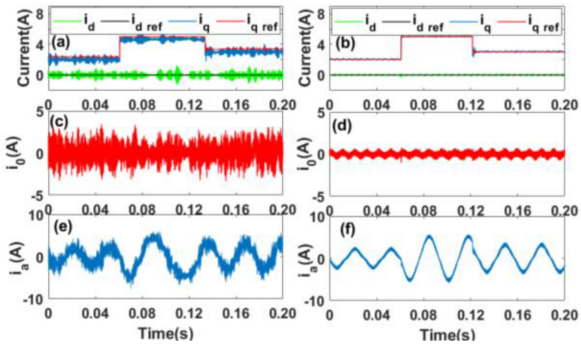

Fig. 13. Simulation results at 500 r/min under $R'_{\rm s}=0.2R_{\rm s}$, $L'_{\rm s}=2L_{\rm s}$, $L'_0=2L_0$, $\Psi'_{3\rm f}=0.25\Psi_{3\rm f}$, $\Psi'_{\rm f}=0.5\Psi_{\rm f}$ condition. (a), (c), and (e) Method 1. (b), (d), and (f) Method 2.

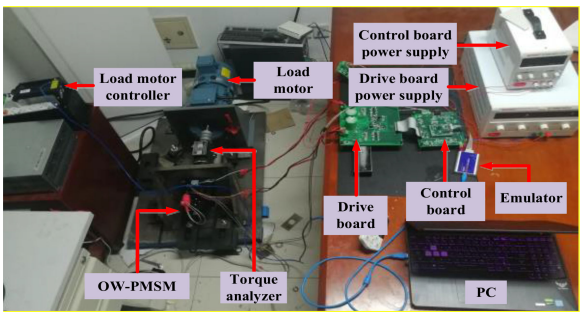

Fig. 14. Experimental platform of OW-PMSM system.

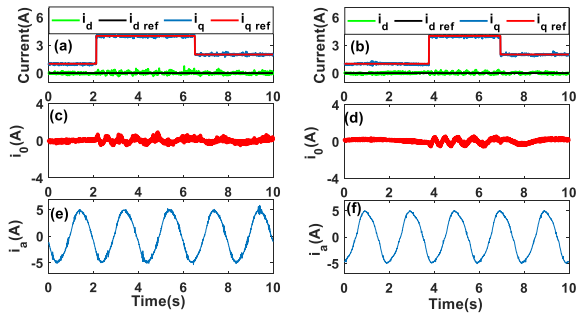

Fig. 15. Experimental results at 500 r/min under no parameter mismatch condition. (a), (c), and (e) Method 1. (b), (d), and (f) Method 2.

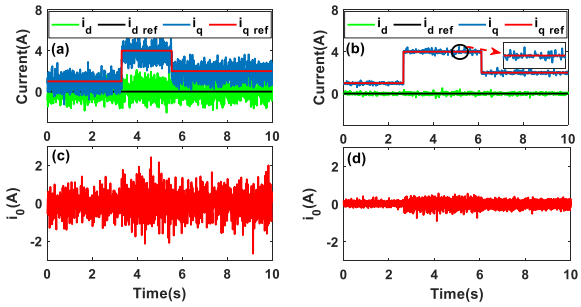

Fig. 16. Experimental results at 200 r/min under $L'_{\rm s}=2L_{\rm s}$ condition. (a) and (c) Method 1. (b) and (d) Method 2.

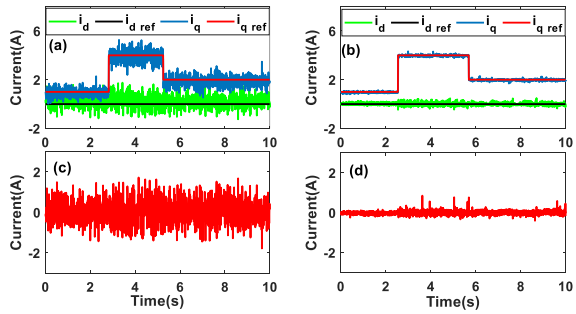

Fig. 17. Experimental results at 300 r/min under $L'_0=2L_0$ condition. (a) and (c) Method 1. (b) and (d) Method 2.

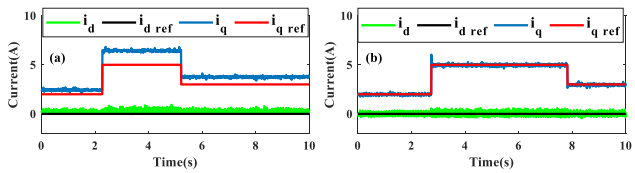

Fig. 18. Experimental results at 400 r/min under $R'_{\rm s}=7R_{\rm s}$ condition. (a) Method 1. (b) Method 2.

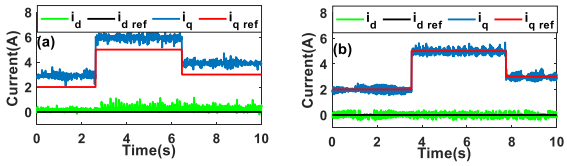

Fig. 19. Experimental results of current at 900 r/min under $\Psi'_{\rm f}=1.5\Psi_{\rm f}$ condition. (a) Method 1. (b) Method 2.

V. Experimental Result

The traditional DPCC control method (Method 1) and the proposed ESO+DPCC control method (Method 2) were also used on the OW-PMSM platform. Fig. 14 shows the OW-PMSM platform, which includes a 1 kW drive OW-PMSM, load motor, power supply (100 V), DSP emulator, and a PC. The main control chip is a TMS320F28337d, and the power module is FNC42060F-type. The sampling frequency is 20 kHz, and the deadtime is set to 2.5 μs. The parameters of OW-PMSM are obtained from the manufacturer's datasheet and the parameters of the ESO are the same as that in the simulation.

Fig. 15 shows the performance of currents $i_{\rm d}$, $i_{\rm q}$, i_0 and the phase current $i_{\rm a}$ of OW-PMSM when there is no parameter mismatch at 500 r/min. The load torque of Fig. 15(a)–(d) ranges from 1 to 4 N·m and from 4 to 3 N·m. The load torque of Fig. 15(e) and (f) is 5 N·m. The two methods are observed to exhibit nearly the same performance.

The experimental results of currents $i_{\rm d}$, $i_{\rm q}$, and i_0 when $L'_{\rm s}=2L_s$ and $L'_0=2L_0$ are shown in Figs. 16 and 17, respectively. Evidently, the current ripples of $i_{\rm d}$ and $i_{\rm q}$ in Method 1 are larger than those in Method 2. In addition, ZSC has worse performance in Method 1. This indicates that the proposed method can suppress inductance mismatch disturbances.

From Figs. 18 and 19, it can be observed that when $R'_{\rm s}=7R_{\rm s}$ or $\Psi'_{\rm f}=1.5\Psi_{\rm f}$, the currents $i_{\rm d}$ and $i_{\rm q}$ in Method 2 can track the

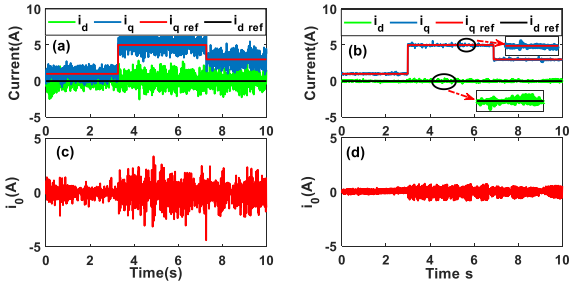

Fig. 20. Experimental results at 300 r/min under $R'_{\rm s} = 4R_{\rm s}$, $L'_{\rm s} = 2L_{\rm s}$, condition. (a) and (c) Method 1. (b) and (d) Method 2.

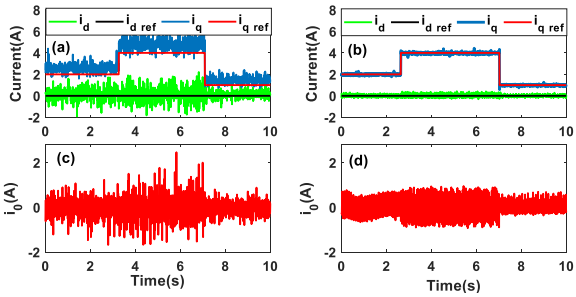

Fig. 21. Experimental results at 400 r/min under $R'_{\rm s} = 5R_{\rm s}$, $L'_{\rm s} = 1.8L_{\rm s}$, $\Psi'_{\rm f} = 2\Psi_{\rm f}$ condition. (a) and (c) Method 1. (b) and (d) Method 2.

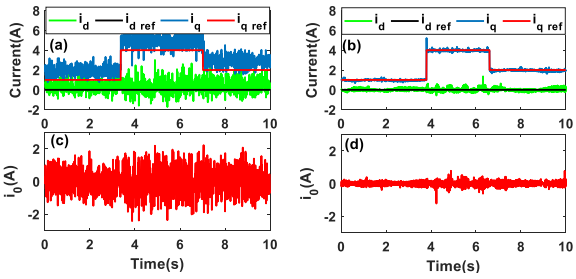

Fig. 22. Experimental results at 500 r/min under $R'_{\rm s} = 0.5R_{\rm s}$, $L'_0 = 2.2L_0$, $\Psi'_{3\rm f} = 2\Psi_{3\rm f}$, condition. (a) and (c) Method 1. (b) and (d) Method 2.

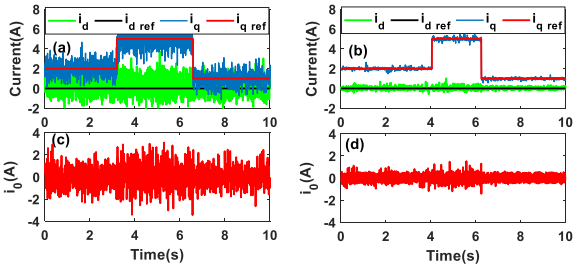

Fig. 23. Experimental results at 600 r/min under $R'_{\rm s} = 1.2R_s$, $L'_s = 2L_{\rm s}$, $L'_0 = 1.5L_0$, $\Psi'_{3\rm f} = 1.5\Psi_{3\rm f}$, condition. (a) and (c) Method 1. (b) and (d) Method 2.

$i_{\rm d}$ reference and $i_{\rm q}$ reference accurately, while those in Method 1 have a significant overshoot.

Figs. 20–24 present the experimental results under a complex situation. Irrespective of the situation, the proposed DPCC+ESO control method exhibits better current performance than Method 1 does, which indicates that the former can suppress a variety of parameter mismatch disturbances.

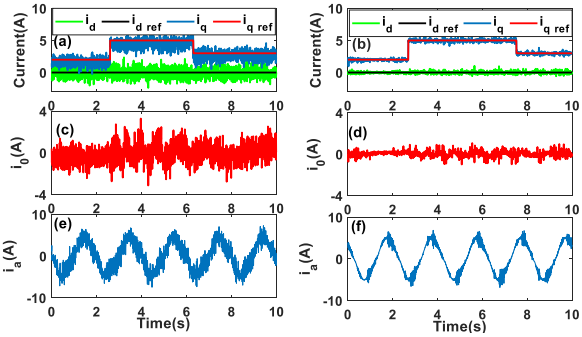

Fig. 24. Experimental results at 500 r/min under $R'_{\rm s} = 0.2R_{\rm s}$, $L'_{\rm s} = 2L_{\rm s}$, $L'_0 = 2L_0$, $\Psi'_{3\rm f} = 0.25\Psi_{3\rm f}$, $\Psi'_{\rm f} = 0.5\Psi_{\rm f}$ condition. (a), (c), and (e) Method 1. (b), (d), and (f) Method 2.

TABLE III
THD (%) OF TWO METHODS UNDER $L'_{\rm s} = 2L_{\rm s}$, $L'_0 = 2L_0$ SITUATION

Speed(r/min)	Method 1	Method 2
200	64.72	27.23
300	58.37	26.43
400	58.07	21.29
500	61.71	17.37
600	57.25	17.14
700	63.02	15.21
800	61.40	14.59
900	69.30	11.48

TABLE IV
$M_{\rm I}$ AND $J_{\rm I}$ OF TWO METHODS UNDER $\Psi'_{\rm f} = 1.5\Psi_{\rm f}$ SITUATION

Speed(r/min)	Method 1		Method 2	
	$M_{\rm i}$	$J_{\rm i}$	$M_{\rm i}$	$J_{\rm i}$
200	0.11	0.14	0.06	0.08
300	0.13	0.16	0.06	0.09
400	0.27	0.29	0.07	0.08
500	0.42	0.43	0.07	0.10
600	0.56	0.27	0.10	0.14
700	0.73	0.73	0.13	0.18
800	0.90	0.91	0.21	0.28
900	1.02	1.03	0.22	0.31

The simulation and experimental results show that inductance has an influence on the harmonic content of the current, while resistance and flux mainly influence the track performance of the current. To enhance the contrast, Tables III –V are presented. Table III lists the total harmonic distortion (THD) of the phase currents of both methods calculated under $L'_{\rm s} = 2L_{\rm s}$ and $L'_0 = 2L_0$ at different speeds. Table IV presents the track performance of the q-axis currents of both methods under $\Psi'_{\rm f} = 1.5\Psi_{\rm f}$. In

TABLE V
THD (%), M_i AND J_i UNDER COMPLEX CONDITION

Condition	Method 1			Method 2		
	THD	M_i	J_i	THD	M_i	J_i
R'_S= 0.5R_S, L'_0=2.2L_0, Ψ'_{3f}=2Ψ_{3f}	48.20	0.93	1.06	8.00	0.07	0.09
R'_S= 1.2R_S, L'_S= 2L_S, L'_0=1.5L_0, Ψ'_{3f}=1.5Ψ_{3f}	112.53	0.63	0.79	24.92	0.07	0.11
R'_S= 0.2R_S, L'_S= 2L_S, L'_0=2L_0, Ψ'_{3f}=0.25Ψ_{3f}, Ψ'_f =0.5Ψ_f	50.50	0.79	0.86	18.15	0.13	0.18

Table V, both THD and track performance are presented under some complex situations. These results clearly demonstrate the effectiveness of the proposed method.

It has to be mentioned that from [33]

$$M_i = \frac{1}{N}\sum_{k=1}^{N}|e_i(k)| = \frac{1}{N}\sum_{k=1}^{N}\left|{i_q}^{\mathrm{ref}}(\mathrm{k}) - i_q(\mathrm{k})\right| \tag{37}$$

$$J_i = \sqrt{\frac{1}{N}\sum_{k=1}^{N}\left({i_q}^{\mathrm{ref}}(\mathrm{k}) - i_q(\mathrm{k})\right)^2}. \tag{38}$$

VI. CONCLUSION

To eliminate the disturbance caused by parameter mismatch in the *d*-axis, *q*-axis, and ZSL, a novel control method, termed ESO+DPCC, which uses OW-PMSM with a common dc bus, is proposed herein. The main conclusions from this article can be presented as follows.

1) ESO can predict the current and disturbance caused by parameter mismatch in the *d*-axis, *q*-axis, and ZSL in the (k+1)th instant, and use them to calculate the (k+1)th instant voltages of the *d*-axis, *q*-axis, and ZSL in DPCC, which can solve the one-step delay problem.
2) ESO can predict the disturbance caused by parameter mismatch in the *d*-axis, *q*-axis, and ZSL, and regard them as feedforward compensation to the traditional DPCC control method to enhance the robustness of the system.
3) From the simulation and experimental results, it can be seen that when there is no parameter mismatch, the traditional DPCC and the proposed ESO+DPCC have similar performances. However, the proposed method is better than the traditional DPCC control method at suppressing the disturbance caused by parameter mismatch, irrespective of whether the mismatch occurs in the *d*-axis, *q*-axis, or ZSL.

The experimental and simulation results prove the robustness of the ESO+DPCC control method under complex situations. Therefore, the proposed ESO+DPCC control method can be experimentally applied to OW-PMSMs drives.

REFERENCES

[1] H. H. Choi, N. T. T. Vu, and J. W. Jung, "Digital implementation of an adaptive speed regulator for a PMSM," *IEEE Trans. Power Electron.*, vol. 26, no. 1, pp. 3–8, Jan. 2011.

[2] X. Lin, W. Huang, and L. Wang, "SVPWM strategy based on the hysteresis controller of zero-sequence current for three-phase open-end winding PMSM," *IEEE Trans. Power Electron.*, vol. 34, no. 4, pp. 3474–3486, Apr. 2019.

[3] Q. An, J. Liu, Z. Peng, L. Sun, and L. Sun, "Dual-space vector control of open-end winding permanent magnet synchronous motor drive fed by dual inverter," *IEEE Trans. Power Electron.*, vol. 31, no. 12, pp. 8329–8342, Dec. 2016.

[4] W. Hu and H. Nian, "Torque ripple suppression method with reduced switching frequency for open-winding PMSM drives with common DC bus," *IEEE Trans. Ind. Electron.*, vol. 66, no. 1, pp. 674–684, Jan. 2019.

[5] H. Zhan, Z. Q. Zhu, M. Odavic, and Y. Li, "A novel zero-sequence model-based sensorless method for open-winding PMSM with common DC bus," *IEEE Trans. Ind. Electron.*, vol. 63, no. 11, pp. 6777–6789, Nov. 2016.

[6] C. Baumann, H. Piquet, X. Roboam, and E. Bru, "A mixed function for actuation and power flow control in embedded networks," *IEEE Trans. Ind. Electron.*, vol. 59, no. 9, pp. 3596–3603, Sep. 2012.

[7] S. Chowdhury, P. W. Wheeler, C. Patel, and C. Gerada, "A multilevel converter with a floating bridge for open-end winding motor drive application," *IEEE Trans. Ind. Electron.*, vol. 63, no. 9, pp. 5366–5375, Sep. 2016.

[8] Z. Shen, D. Jiang, L. Zhu, and T. Zou, "A novel zero-sequence current elimination PWM scheme for an open-winding PMSM with common DC bus," *IEEE Trans. Power Electron.*, vol. 34, no. 12, pp. 12476–12490, Dec. 2019.

[9] Z. Gao, D. Jiang, and W. Kong, "A GaN-based integrated modular motor drive for open-winding permanent magnet synchronous motor application," in *Proc. Workshop Wide Bandgap Power Devices Appl. Asia*, China, May 2017, pp. 73–79.

[10] K. V. P. Kumar and T. V. Kumar, "Improvised direct torque control strategies of open-end winding PMSM fed with multi-level inversion," in *Proc. IEEE Int. Conf. Ind. Technol.*, France, Feb. 2018, pp. 425–430.

[11] X. Zhang, L. Sun, and K. Zhao, "Nonlinear speed control for PMSM system using sliding-mode control and disturbance compensation technique," *IEEE Trans. Power Electron.*, vol. 28, no. 3, pp. 1358–1365, Mar. 2013.

[12] N. Hunter, T. Cox, P. Zanchetta, and S. A. Odhano, "Torque quality improvement of an open-end winding PMSM," in *Proc. IEEE Energy Convers. Congr. Expo.*, Portland, Sep. 2018, pp. 4254–4261.

[13] C. Sun, D. S. Un, Z. Zheng, and H. Nian, "Simplified model predictive control for dual inverter-fed open-winding permanent magnet synchronous motor," *IEEE Trans. Energy Convers.*, vol. 33, no. 4, pp. 1846–1854, Dec. 2018.

[14] X. Yuan, C. Zhang, and S. Zhang, "A novel deadbeat predictive current control scheme for OEW-PMSM drives," *IEEE Trans. Power Electron.*, vol. 34, no. 12, pp. 11990–12000, Dec. 2019.

[15] S. Kouro, P. Cortés, and R. Vargas, "Model predictive control—A simple and powerful method to control power converters," *IEEE Trans. Ind. Electron.*, vol. 56, no. 6, pp. 1826–1838, Jun. 2009.

[16] Z. Mynar, L. Vesely, and P. Vaclavek, "PMSM model predictive control with field-weakening implementation," *IEEE Trans. Ind. Electron.*, vol. 63, no. 8, pp. 55156–55126, Aug. 2016.

[17] S. Vazquez, J. Rodriguez, and M. Rivera, "Model predictive control for power converters and drives: Advances and trends," *IEEE Trans. Ind. Electron.*, vol. 64, no. 2, pp. 935–947, Feb. 2017.

[18] R. C. Kim and S. Kwak, "Model predictive control method for CHB multilevel inverter with reduced calculation complexity and fast dynamics," *IET Electric Power Appl.*, vol. 11, no. 5, pp. 784–792, May 2017.

[19] S. Chowdhury, P. Wheeler, Z. Huang, M. Rivera, and C. Gerada, "Fixed switching frequency predictive control of an asymmetric source dual inverter system with a floating bridge for multilevel operation," *IET Power Electron.*, vol. 12, no. 3, pp. 450–457, Mar. 2019.

[20] A. A. Ahmed, J. Kim, and Y. Lee, "Model predictive torque control of PMSM for EV drives: A comparative study of finite control set and predictive deadbeat control schemes," in *Proc. Int. Middle East Power Syst. Conf.*, Egypt, Dec. 2016, pp. 156–163.

[21] W. Song, Z. Deng, S. Wang, and X. Feng, "A simple model predictive power control strategy for single-phase PWM converters with modulation function optimization," *IEEE Trans. Power Electron.*, vol. 31, no. 7, pp. 5279–5289, Jul. 2016.
[22] A. Abbaszadeh, M. A. Miremadi, D. A. Khaburi, and M. Esmaeili, "Permanent synchronous motor predictive deadbeat current control-robustness investigation," in *Proc. Power Electron., Drive Syst. Technologies Conf.*, Iran, 2015, pp. 406–411.
[23] M. Siami, D. A. Khaburi, A. Abbaszadeh, and J. Rodríguez, "Robustness improvement of predictive current control using prediction error correction for permanent-magnet synchronous machines," *IEEE Trans. Ind. Electron.*, vol. 63, no. 6, pp. 3458–3466, Jun. 2016.
[24] S. Bibian and H. Jin, "Time delay compensation of digital control for DC switchmode power supplies using prediction techniques," *IEEE Trans. Power Electron.*, vol. 15, no. 15, pp. 835–842, Sep. 2000.
[25] T. Türker, U. Buyukkeles, and A. F. Bakan, "A robust predictive current controller for PMSM drives," *IEEE Trans. Ind. Electron.*, vol. 63, no. 6, pp. 3906–3914, Jun. 2016.
[26] M. Yang, X. Lang, J. Long, and D. Xu, "Flux immunity robust predictive current control with incremental model and extended state observer for PMSM drive," *IEEE Trans. Power Electron.*, vol. 32, no. 12, pp. 9267–9279, Dec. 2017.
[27] L. He, F. Wang, J. Wang, and J. Rodríguez, "Zynq implemented luenberger disturbance observer based predictive control scheme for PMSM drives," *IEEE Trans. Power Electron.*, vol. 35, no. 2, pp. 1770–1778, Feb. 2020.
[28] Y.A-R.I. Mohamed, "Design and implementation of a robust current-control scheme for a PMSM vector drive with a simple adaptive disturbance observer," *IEEE Trans. Power Electron.*, vol. 54, no. 4, pp. 1981–1988, Aug. 2007.
[29] X. Zhang, B. Hou, and Y. Mei, "Deadbeat predictive current control of permanent-magnet synchronous motors with stator current and disturbance observer," *IEEE Trans. Power Electron.*, vol. 32, no. 5, pp. 3818–3834, May 2017.
[30] V. T. Somasekhar, S. Srinivas, and B. R. Prakash, "Pulse width-modulated switching strategy for the dynamic balancing of zero-sequence current for a dual-inverter fed open-end winding induction motor drive," *IET Electric Power Appl.*, vol. 1, no. 4, pp. 591–600, Jul. 2007.
[31] Y. Zhou and H. Nian, "Zero-sequence current suppression strategy of open-winding PMSG system with common DC bus based on zero vector redistribution," *IEEE Trans. Ind. Electron.*, vol. 62, no. 6, pp. 3399–3408, Jun. 2015.
[32] A. H. M. Sayem, Z. Cao, and Z. Man, "Model free ESO-based repetitive control for rejecting periodic and aperiodic disturbances," *IEEE Trans. Ind. Electron.*, vol. 64, no. 4, pp. 3433–3441, Apr. 2017.
[33] C. K. Lin, J. T. Yu, Y. S. Lai, and H. C. Yu, "Improved model-free predictive current control for synchronous reluctance motor drives," *IEEE Trans. Ind. Electron.*, vol. 63, no. 6, pp. 3942–3953, Jun. 2016.

Xueping Li was born in Shan dong, China, in 1994. He received the B.Eng. degree in vehicle engineering from the Chang'an University, Xi'an, China, in 2018. He is currently working toward the Ph.D. degree with the National Engineering Laboratory for Electric Vehicles, School of Mechanical Engineering, Beijing Institute of Technology, Beijing, China.

His research interests include predictive control for synchronous motor drives and multiphase motor drives.

Shuo Zhang (Member, IEEE) received the B.Eng. degree from North China Institute of Aerospace Engineering, Hebei, China, in 2011, and the Ph.D. degree in vehicle engineering from the Beijing Institute of Technology, Beijing, China, in 2017.

He is currently an Assistant Professor with the National Engineering Laboratory for Electric Vehicles, School of Mechanical Engineering, Beijing Institute of Technology. His research interests include the modeling and control for the permanent magnet synchronous motors, multimotor driving systems, and hybrid power systems.

Chengning Zhang received the M.E. degree in control theory and control engineering and the Ph.D. degree in vehicle engineering from the Beijing Institute of Technology, Beijing, China, in 1989 and 2001, respectively.

He is currently a Professor and the Vice Director with the National Engineering Laboratory for Electric Vehicles, Beijing Institute of Technology. His research interests include electric vehicles, vehicular electric motor drive systems, battery management systems, and chargers.

Ying Zhou was born in Hebei, China, in 1997. She received the B.Eng. degree in vehicle engineering from the Dalian University of Technology, Dalian, China, in 2018. She is currently working toward the Ph.D. degree with the National Engineering Laboratory for Electric Vehicles, School of Mechanical Engineering, Beijing Institute of Technology, Beijing, China.

Her research interests include synchronous motor drives, open winding permanent magnet synchronous motor drives, and parameter identification strategy of motors.

Chuntao Zhang was born in Shandong, China, in 1996. He received the B.Eng. degree in vehicle engineering from the Harbin Institute of Technology, Harbin, China, in 2014. He is currently working toward the Ph.D. degree with the Collaborative Innovation Center for Electric Vehicles, School of Mechanical Engineering, Beijing Institute of Technology, Beijing, China.

His research interests include the control for the permanent magnet synchronous motors and data-driven forecasting with applications to automated and connected vehicles.